A Panoramic System for Vibration Analysis

Jeffrey L. Lindner
Structures and Dynamics Laboratory
George C. Marshall Space Flight Center
Marshall Space Flight Center, Alabama 35812

John A. Gilbert
Department of Mechanical and Aerospace Engineering
University of Alabama in Huntsville
Huntsville, Alabama 35899

ABSTRACT

This paper describes a method for capturing time-average holograms using a panoramic imaging system. It includes the development of the phase-displacement relation required to analyze the interference fringe patterns, and a discussion of the modulation in the sensitivity vector across the inner walls of an aluminum ring and a turbopump liner.

1 INTRODUCTION

Prior research, conducted on interior curved surfaces using the method of panoramic time-average holo-interferometry, has demonstrated the utility of panoramic annular lenses (PALs).[1,2] Discussions regarding the governing equations and the modulation of the sensitivity vector over the region of interest were included in these papers but the corresponding analyses were based on complex ray traces and performed using computational techniques. Since no parametric equations were provided to quantify the approach, it was difficult for potential users to apply the method, especially when designing and characterizing alternative optical setups. A solution to this problem was found when the imaging characteristics of a PAL were expressed in closed form.[3]

2 HOLO-INTERFEROMETRIC RECORDING SYSTEM

Figure 1 shows a schematic diagram of a holographic system that is currently being used by NASA to visualize the mode shapes of cylindrically shaped structural components typically found in rocket engines. Two 38 mm (1.5 in.) diameter PALs are aligned and positioned at a known distance apart within the cylindrical cavity. The inner wall of the structural component is illuminated with coherent light by passing a collimated beam through the illuminating PAL.

The illuminated surface is captured by the imaging PAL, and a time average hologram of the wavefronts emerging from this lens is recorded using a thermoplastic holocamera positioned behind a collector lens. Since the test object is allowed to execute many cycles of steady vibration while the hologram is being recorded, the holographic reconstruction reveals contours of constant amplitude.

The intensity of the reconstructed image is given by[4]

$$I \propto J_o^2 \left[\frac{2\pi}{\lambda} \{(\hat{\mathbf{e}}_I - \hat{\mathbf{e}}_V) \cdot \mathbf{d}\}\right] = J_o^2 \left[\frac{2\pi}{\lambda} (\mathbf{C} \cdot \mathbf{d})\right] \quad (1)$$

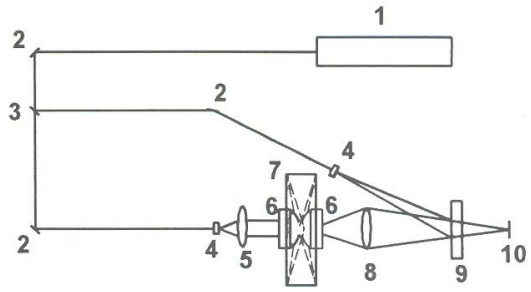

***Figure 1**. Experimental setup; 1. laser, 2, mirror, 3. beam splitter, 4. spatial filter, 5. collimating lens, 6. PAL, 7. test object, 8. transfer lens, 9. thermoplastic plate, 10. image plane on CCD camera.*

where λ is the wavelength of the coherent light used to record and reconstruct the hologram, $\mathbf{d}$ is the displacement vector of the surface point under consideration, and J_o is the zero order Bessel function. The vectors $\hat{\mathbf{e}}_I$ and $\hat{\mathbf{e}}_V$ are unit vectors in the directions of illumination and observation, respectively; and, $\mathbf{C} = (\hat{\mathbf{e}}_I - \hat{\mathbf{e}}_V)$ is the sensitivity vector along which the displacement vector $\mathbf{d}$ is projected.

Figure 2 shows one of the 36 panoramic holo-interferometric images acquired during a modal analysis performed on a turbopump liner designed for use in NASA's Space Shuttle Main Engine.[2] The first quadrant of the image is linearized to remove radial and circumferential distortions. The innermost portion of the annulus, and the top of the linearized image, correspond to the stiff (flange) end of the inlet while the outermost portion of the annulus, and the bottom of the linearized image, correspond to the soft end. In this case, the fringes represent peak-to-peak radial displacement.

When the displacement is zero, the reconstructed image is the brightest; consequently, regions having no motion, or nodes in the vibratory pattern, exhibit the greatest intensity. Dark fringes occur at the roots (zeros) of J_o^2; the particular root on the interferogram may be determined by counting from the nearest stationary point on the object, marked by the very bright fringe corresponding to the nodal location. The roots of J_o are tabulated and these values may be used together with the known values of the sensitivity vector to determine the amplitude of the object motion in the direction

of the sensitivity vector. A detailed analysis of the interferometric system and its sensitivity to various displacement components follows.

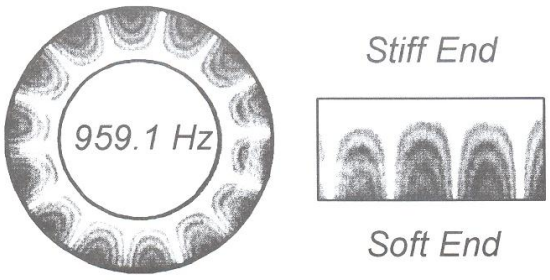

***Figure 2**. A panoramic holo-interferogram; and, a linearized image of the first quadrant.*

3 SYSTEM CHARACTERIZATION

Figure 3 shows two PALs located within a section of cylindrical pipe of radius, R. The entrance pupil center of the PAL used to illuminate the surface is offset a distance of z_e = 6.74 mm (0.26 in.) toward the front of the lens, and y_e = 1.34 mm (0.05 in.) from the optical axis (for object points contained in the Y,Z plane). The angular field of view measured from this point is 45.4° covering the range -18.8° ≤ φ_i ≤ 26.6°, where φ_i is the field angle. By convention, positive field angles are measured toward the front of the lens.

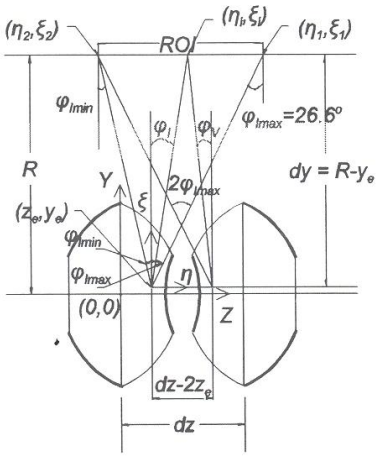

***Figure 3**. Nomenclature for a dual PAL system.*

The illuminating PAL produces a circumferential belt on the inner wall of the pipe. The linear distance that is illuminated by the first lens is defined as the field of view (FOV). For a 38 mm (1.5 in.) diameter PAL,[3]

$$FOV = (R - y_e)(\tan 26.6^\circ + \tan 18.8^\circ) \quad . \qquad (2)$$

The imaging PAL has similar optical characteristics and captures a portion of the illuminated surface. When a coherent light source is used and a reference beam added, interference occurs over a region of interest (ROI) where the beams overlap. The length of the ROI is[3]

$$ROI = 2 \tan \varphi_{l_{max}} \left(R - y_e - \frac{dz - 2z_e}{2 \tan \varphi_{l_{max}}}\right) \qquad (3)$$

where φ_{lmax} is equal to 26.6° for the 38 mm (1.5 in.) diameter PALs shown in Fig. 3, (y_e,z_e) is the location of the entrance pupil center of the illuminating PAL measured with respect to an axes system located at its center (0,0), R-y_e = dy, dz is the lens spacing measured between the centerlines of the lenses, and R is the radius of the pipe (or the object distance measured perpendicular to the optical axis from the center of the PAL).

The ROI extends from φ_{lmax} = 26.6° to a minimum field angle, φ_{lmin}, given by

$$\varphi_{l_{min}} = \tan^{-1}\left[\frac{dz - 2z_e - (R - y_e)\tan \varphi_{l_{max}}}{R - y_e}\right] \quad . \qquad (4)$$

The field angle corresponding to the center of the ROI, φ_C, is given by

$$\varphi_{l_c} = \tan^{-1}\left[\frac{(R - y_e)\tan \varphi_{l_{max}} - \frac{ROI}{2}}{R - y_e}\right] \qquad (5)$$

where ROI is the length computed from Eqn. (3).

A pipe section having a length, L, that is smaller than the ROI, is usually centered within the region of interest. In this case, the field angles corresponding to the extremities are given by

$$\varphi_{l_{front,back}} = \tan^{-1}\left[\frac{(R - y_e)\tan \varphi_{l_{max}} - \frac{ROI}{2} \pm \frac{L}{2}}{R - y_e}\right] \qquad (6)$$

where the "+" and "-" signs are associated with the right and left edges of the section, respectively.

The field angles measured relative to the imaging lens, φ_V, can be computed from the field angles measured relative to the illuminating lens, φ_l, using

$$\varphi_V = \tan^{-1}\left[\frac{dz - 2z_e - (R - y_e)\tan \varphi_l}{R - y_e}\right] \quad . \qquad (7)$$

In Eqns. (2) through (7), the radius and lens spacing are the only variables present. They depend on the optical setup and the geometry of the object under consideration.

4 SENSITIVITY CONSIDERATIONS

Not all the rays exiting or entering the lens actually pass through the entrance pupil center, so a linear regression was performed on ray trace data to establish a parametric equation describing the direction of propagation of the

illuminating wavefront, given by the angle γ_i, in terms of the field angle, φ_i.[3] For a plane wavefront entering the flat surface of the PAL,[3]

$$\gamma_i = 1.00417\ \varphi_i - 0.2978 \qquad (8)$$

where both angles are measured in degrees from a local coordinate system (η,ξ) introduced at the entrance pupil center.

As illustrated in Fig. 4, the sensitivity vector included in Eqn, (1) lies in the plane formed by the illumination and observation vectors, and is directed along their angle bisector. The unit vectors, $\hat{\mathbf{e}}_I$ and $\hat{\mathbf{e}}_V$ may be described in terms of the directions of propagation of the illuminating and viewing wavefronts as

$$\hat{\mathbf{e}}_I = \cos\gamma_I\, \boldsymbol{j} + \sin\gamma_I\, \boldsymbol{k} \qquad (9)$$

and

$$\hat{\mathbf{e}}_V = -\cos\gamma_V\, \boldsymbol{j} + \sin\gamma_V\, \boldsymbol{k} \qquad (10)$$

respectively. Thus, the sensitivity vector may be expressed as

$$\begin{aligned} \boldsymbol{C} &= C_y\, \boldsymbol{j} + C_z\, \boldsymbol{k} \\ &= (\cos\gamma_I + \cos\gamma_V)\, \boldsymbol{j} + (\sin\gamma_I - \sin\gamma_V)\, \boldsymbol{k} \ . \end{aligned} \qquad (11)$$

The displacement vector can be expressed in terms of its scalar components as

$$\boldsymbol{d} = u\, \boldsymbol{i} + v\, \boldsymbol{j} + w\, \boldsymbol{k} \ . \qquad (12)$$

Equations (11) and (12) can be used to quantify the projected displacement in Eqn. (1) as

$$\begin{aligned} \boldsymbol{C} \cdot \boldsymbol{d} &= C_y v + C_z w \\ &= (\cos\gamma_I + \cos\gamma_V)\, d\cos\gamma_d \\ &\quad + (\sin\gamma_I - \sin\gamma_V)\, d\sin\gamma_d \end{aligned} \qquad (13)$$

where d is the magnitude of the displacement vector and γ_d is the angle that the displacement vector makes with respect to the positive Y axis. Since Eqn. (8) holds for both lenses, Eqn. (13) can be rewritten as

$$\begin{aligned} \boldsymbol{C} \cdot \boldsymbol{d} &= [\cos(1.00417\varphi_I - 0.2978) \\ &\quad + \cos(1.00417\varphi_V - 0.2978)]\, d\cos\gamma_d \\ &\quad + [\sin(1.00417\varphi_I - 0.2978) \\ &\quad + \sin(1.00417\varphi_V - 0.2978)]\, d\sin\gamma_d \end{aligned} \qquad (14)$$

where φ_V is given in terms of φ_I via Eqn. (7).

Although the derivation was performed by considering the Y,Z plane, the problem is radially symmetric. Since the terms (d cos γ_d) and (d sin γ_d) represent the out-of-plane (radial) and in-plane (longitudinal) displacement components, respectively, there is no sensitivity to circumferential displacement.

Sections 5 and 6 show how these parametric equations can be applied to characterize the optical systems described in References 1 and 2, respectively.

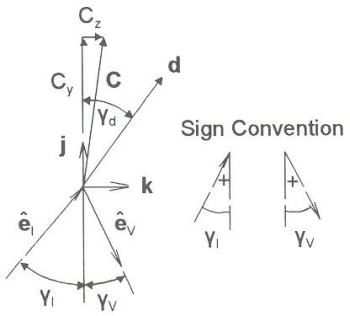

***Figure 4**. The sensitivity vector, **C**, has an out-of-plane (radial) component, C_y, and an in-plane (longitudinal) component, C_z.*

5 AN ALUMINUM RING

In Reference 1, a panoramic recording system was used to study the modal response of a 1.27 mm (0.05") thick, 2.13 cm (0.84") long, aluminum ring having an outside diameter of 10.16 cm (4.00"). The ring was supported radially at each end by 8 elastic bands spaced at 45° intervals around the circumference. It was positioned around the PALs with its longitudinal axis along z. The lenses were separated at a distance, dz = 25.4 mm (1 in.) apart The inner surface of the ring was painted white. Coherent light from a 400 milliwatt Argon-ion laser (λ = 514 nm) was projected onto the inner wall by expanding and collimating the object beam, and then passing the collimated beam through one of the PALs. Eighteen panoramic holo-interferograms of in-plane flexural modes due to twisting and/or bending were acquired as the ring was acoustically excited.

Since the ring's inner wall is located 49.53 mm (1.95 in.) from the Z axis, and y_e = 1.34 mm (0.05 in.), Eqn. (2) predicts a field of view equal to 40.54 mm (1.6 in.). The ROI is slightly smaller; Eqn. (3) predicts it to extend over 36.34 mm (1.43 in.) based on the values: dz = 25.4 mm (1.0 in.); φ_{Imax} = 26.6°; and, z_e = 6.74 mm (0.26 in.). The minimum field angle associated with the ROI is computed from Eqn. (4) as φ_{Imin} = -14.2°.

Figure 5 shows a plot of the out-of-plane (radial) sensitivity coefficient, C_y, versus the field angle over the ROI. Since matched viewing and illuminating wavefronts are used, the direction of the sensitivity vector changes in a symmetric fashion about the center of the ROI [corresponding to φ_C = 7.02°; and, obtained from Eqn. (5)], and the plot is symmetrical. The data shows that C_y remains fairly constant over the ROI with a maximum of 1.986 at $\varphi_I = \varphi_C$ = 7.02°. The deviation from this value is 6.2% for the 25.4 mm (1.0 in.) lens spacing and 49.53 mm (1.95 in.) object distance employed. Since the length of the ring [2.13 cm (0.84 in.)] is smaller than the ROI; the deviation is only 2.2% over the inner surface when the ring is centered [$-5.6° \le \varphi_I \le 19.0°$; a range obtained from Eqn. (6)].

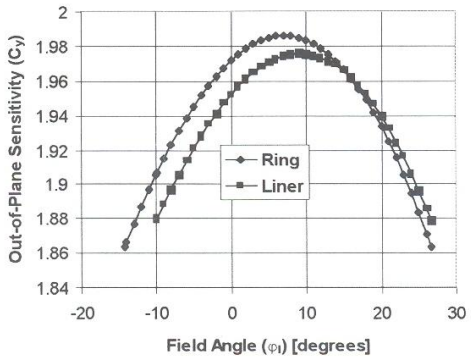

Figure 5. Out-of-plane sensitivity coefficient.

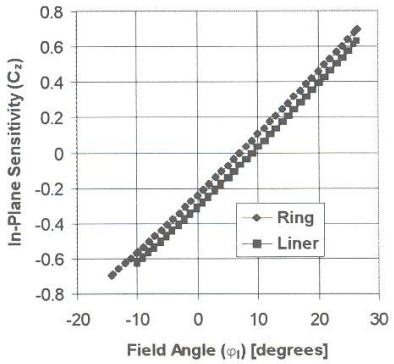

Figure 6. In-plane sensitivity coefficient.

The in-plane (longitudinal) sensitivity coefficient, C_z , is plotted in Fig. 6. The plot is nearly linear; the sensitivity to this component is significant at points located at the edges of the ROI and goes to zero at the center. At points on the edges of the ROI, corresponding to $\varphi_{Imax} = 26.6°$ and $\varphi_{Imin} = -14.2°$, the phase change incorporates 70% of the longitudinal displacement component. At the edges of the ring, the value is 42%.

6 A TURBOPUMP LINER

In Reference 2, a panoramic recording system was used to study the modal response of a turbopump liner designed for use in NASA's Space Shuttle Main Engine. The 8.9 cm (3.5 in.) long Incoloy 909 liner was fabricated with a flange at one end on its outer surface; the inner surface was cylindrical with an inner diameter of 280 mm (11.0 in.).

During the tests, the liner was supported by four foam blocks and 27 elastic cords to provide a free-free boundary condition. It was positioned around the PALs with its longitudinal axis along z. The lenses were separated at a distance, dz = 58.58 mm (2.3 in.) apart The inner surface of the liner was painted white. Coherent light from a 400 milliwatt Argon-ion laser (λ = 514 nm) was projected onto the wall by expanding and collimating the object beam, and then passing the collimated beam through one of the PALs. Figure 2 shows a typical mode shape captured as the liner was acoustically excited.

Since the liner's wall is located 140 mm (5.5 in.) from the Z axis and y_e = 1.34 mm (0.05 in.), Eqn. (2) predicts a field of view equal to 116.6 mm (4.6 in.). The ROI is slightly smaller; Eqn. (3) predicts it to extend over 93.8 mm (3.7 in.) based on the values: dz = 58.58 mm (2.3 in.); $\varphi_{Imax} = 26.6°$; and, z_e = 6.74 mm (0.26 in.). The minimum field angle associated with the ROI is computed from Eqn. (4) as $\varphi_{Imin} = -10°$.

Figure 5 shows a plot of the out-of-plane (radial) sensitivity coefficient, C_y, versus the field angle over the ROI. Since matched viewing and illuminating wavefronts are used, the direction of the sensitivity vector changes in a symmetric fashion about the center of the ROI [corresponding to $\varphi_C = 9.15^0$; and, obtained from Eqn. (5)], and the plot is symmetrical. The data shows that C_y remains fairly constant over the ROI with a maximum of 1.976 at $\varphi_I = \varphi_C = 9.15^0$. The deviation from this value is 4.9% for the 58.58 mm (2.3 in.) lens spacing and 140 mm (5.5 in.) object distance employed. Since the length of the liner [8.9 cm (3.5 in.)] is only slightly smaller than the ROI; the deviation is 4.4% over the inner surface when the liner is centered [$-9.3° \le \varphi_I \le 25.6°$; a range obtained from Eqn. (6)].

The in-plane (longitudinal) sensitivity coefficient, C_z , is plotted in Fig. 6. The plot is nearly linear; the sensitivity to this component is significant at points located at the edges of the ROI and goes to zero at the center. At points on the edges of the ROI, corresponding to $\varphi_{Imax} = 26.6°$ and $\varphi_{Imin} = -10°$, the phase change incorporates 63% of the longitudinal displacement component. At the edges of the liner, the value is 59%.

7 ACKNOWLEDGMENT

Panoramic lenses were secured from Optechnology, Inc., located in Gurley, Alabama.

REFERENCES

[1] **Lindner, J.L., Gilbert, J.A.**, "Modal analysis using time-average panoramic holo-interferometry," *Modal Analysis: The International Journal of Analytical and Experimental Modal Analysis*, 10(3): 143-151 (1995).

[2] **Lindner, J.L., Gilbert, J.A.**, "Panoramic modal testing of the Space Shuttle Main Engine alternative turbopump inlet bellows liner," *Exp. Techniques*, 22 (2): 15-19 (1998).

[3] **Matthys, D.R., Gilbert, J.A., Fair, S.B.**, "Characterization of optical systems for radial metrology," *Proc. of the SEM IX International Congress on Experimental Mechanics*, June 5-8, 2000.

[4] **Stetson, K.A., Powell, R.L.**, "Interferometric hologram evaluation and real time vibration analysis of diffuse objects," *J. Opt. Soc. of Am.*, 55: 1694-1695 (1965).